Supplemental Material: Possible high T_c superconductivity in $La_3Ni_2O_7$ under high pressure through manifestation of a nearly-half-filled bilayer Hubbard model

Hirofumi Sakakibara,[1,2,*] Naoya Kitamine,[3] Masayuki Ochi,[3,4] and Kazuhiko Kuroki[3]

[1] *Advanced Mechanical and Electronic System Research Center(AMES), Faculty of Engineering, Tottori University, 4-10 Koyama-cho, Tottori, Tottori 680-8552, Japan*

[2] *Computational Condensed Matter Physics Laboratory, RIKEN, Wako, Saitama 351-0198, Japan*

[3] *Department of Physics, Osaka University, 1-1 Machikaneyama-cho, Toyonaka, Osaka 560-0043, Japan*

[4] *Forefront Research Center, Osaka University, 1-1 Machikaneyama-cho, Toyonaka, Osaka 560-0043, Japan*

(Dated: December 22, 2023)

I. DETAILS OF MODEL CONSTRUCTION

As shown in the main text of the Letter, we have performed first-principles calculation to obtain the band structure of $La_3Ni_2O_7$, using the crystal structure parameters summarized in Tab. S1. We adopt the theoretically optimized atomic positions given in the lower part ($P = 29.5$ GPa case) of the Extended Data Table 1 in Ref. [S1], while we use tetragonalized in-plane lattice constants $a^* = b^* = (a+b)/2\sqrt{2} = (5.289\,\text{Å} + 5.218\,\text{Å})/2\sqrt{2} = 3.715$ Å, where a and b are the experimental lattice constants given in Ref. [S1] for space group $Fmmm$. Comparison between the band structures of the original crystal structure with $Fmmm$ symmetry and that of the tetragonalized structure is shown in Fig. S1. Adopting tetragonal symmetry is further justified in recent experimental [S2] and theoretical studies [S3, S4], which finds $I4/mmm$ structural symmetry at high pressures at which superconductivity is realized.

TABLE S1. Structural parameters adopted in the first-principles calculation. Here, O(1) is the in-plane oxygen, O(2)/O(3) are the outer/inner apical oxygens. The in-plane lattice constants a^* and b^* are those for tetragonal symmetry obtained by averaging the original value of a, b in Ref. [S1].

Space group: $I4/mmm$			
$a^* = b^* = 3.715$ Å, $c = 19.734$ Å, $\alpha = \beta = \gamma = 90^\circ$			
atom	x	y	z
La(1)	0	0	0.321
La(2)	0	0	0.5
Ni	0	0	0.096
O(1)	0.5	0	0.095
O(2)	0	0	0.204
O(3)	0	0	0

After first-principles calculation in the way described in the main text, we construct the maximally localized Wannier functions [S5, S6] by using the RESPACK code [S7–S13] to obtain the hopping parameters among the Wannier functions. We set the two orbitals having $d_{x^2-y^2}$ and $d_{3z^2-r^2}$ symmetry per two Ni sites as a initial guess of Wannier functions. The adopted parameters of energy windows [S14] are summarized in Tab. S2 and depicted in Fig. S2.

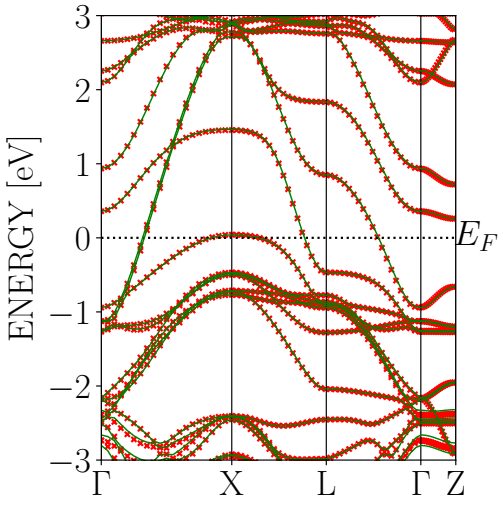

FIG. S1. Comparison between the band structures of the original crystal structure with $Fmmm$ symmetry [S1] (green solid line) and that of the tetragonalized structure (red cross). Both band structures are presented in the Brillouin zone of the face-centered orthorhombic lattice.

TABLE S2. The parameters of energy windows [S14] adopted in the Wannierization process measured from the Fermi energy.

[eV]	
Upper energy window	3.25
Upper inner window	0.65
Lower inner window	-0.26
Lower energy window	-1.56

II. FLUCTUATION EXCHANGE APPROXIMATION

In our study, we adopt the fluctuation exchange (FLEX) approximation to take into account the correlation effects beyond those in the first principles calculation, and also to analyze the possibility of unconventional superconductivity originating from spin fluctua-

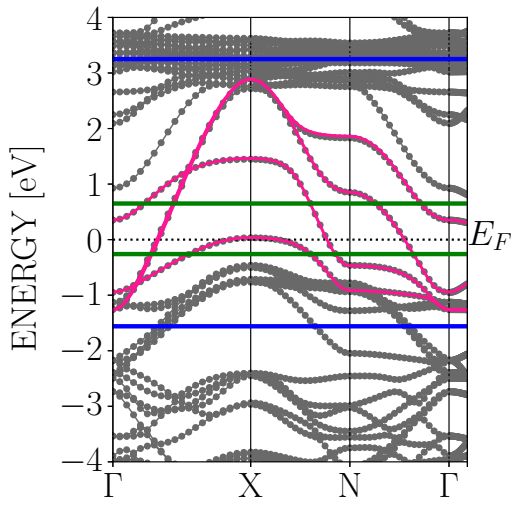

FIG. S2. The positions of energy windows [S14] are superposed on Fig.1(c) of the main text. Blue/green lines indicate energy/inner windows.

tions. Here we describe the FLEX formalism. We consider a multi-orbital Hamiltonian given in the present form,

$$\begin{aligned} H_{\rm int} = \; & U\sum_{i,\mu} n_{i\mu\uparrow}n_{i\mu\downarrow} + U'\sum_{i,\mu<\nu,\sigma} n_{i\mu\sigma}n_{i\nu\bar{\sigma}} \\ & +(U'-J)\sum_{i,\mu<\nu,\sigma} n_{i\mu\sigma}n_{i\nu\sigma} \\ & -J\sum_{i,\mu\neq\nu} c^\dagger_{i\mu\uparrow}c_{i\mu\downarrow}c^\dagger_{i\nu\downarrow}c_{i\nu\uparrow} \\ & +J'\sum_{i,\mu\neq\nu} c^\dagger_{i\mu\uparrow}c^\dagger_{i\mu\downarrow}c_{i\nu\downarrow}c_{i\nu\uparrow}. \end{aligned} \tag{S1}$$

Here, U, U', J, and J' are the intraorbital repulsion, the interorbital repulsion, Hund's coupling, and the pair hopping, respectively. i denotes the sites, μ, ν the orbitals, and σ the spins. $c_{i\mu\sigma}$ and $c^\dagger_{i\mu\sigma}$ are annihilation and creation operators of electrons, respectively, and $n_{i\mu\sigma} = c^\dagger_{i\mu\sigma}c_{i\mu\sigma}$.

In the FLEX approximation, the self energy is calculated by taking into account the bubble and ladder type diagrams that comprise the irreducible susceptibility

$$\chi^0_{l_1l_2l_3l_4}(q) = -\frac{T}{N}\sum_k G_{l_3l_1}(k)G_{l_2l_4}(k+q), \tag{S2}$$

which is calculated from the renormalized Green's function G, where q stands for both the wave vector and the Matsubara frequency, and l_i denotes the orbitals. The renormalized Green's function is calculated from the Dyson equation, and hence obtained in a self-consistent manner. Using the converged Green's function and the spin and charge susceptibilities,

$$\hat{\chi}_s(q) = \frac{\hat{\chi}^0(q)}{1-\hat{S}\hat{\chi}^0(q)}, \tag{S3}$$

$$\hat{\chi}_c(q) = \frac{\hat{\chi}^0(q)}{1+\hat{C}\hat{\chi}^0(q)}, \tag{S4}$$

respectively, with the interaction matrices

$$S_{l_1l_2l_3l_4} = \begin{cases} U, & l_1=l_2=l_3=l_4, \\ U', & l_1=l_3\neq l_2=l_4, \\ J, & l_1=l_2\neq l_3=l_4, \\ J', & l_1=l_4\neq l_2=l_3, \end{cases} \tag{S5}$$

$$C_{l_1l_2l_3l_4} = \begin{cases} U, & l_1=l_2=l_3=l_4, \\ -U'+J, & l_1=l_3\neq l_2=l_4, \\ 2U'-J, & l_1=l_2\neq l_3=l_4, \\ J', & l_1=l_4\neq l_2=l_3, \end{cases} \tag{S6}$$

the effective spin-singlet pairing interaction

$$\hat{\Gamma}(q) = \frac{3}{2}\hat{S}\hat{\chi}_s(q)\hat{S} - \frac{1}{2}\hat{C}\hat{\chi}_c(q)\hat{C} + \frac{1}{2}(\hat{S}+\hat{C}) \tag{S7}$$

is obtained, which is plugged into the linearized Eliashberg equation to analyze superconductivity,

$$\begin{aligned} & \lambda\Delta_{\mu\nu}(k) \\ & = -\frac{T}{N}\sum_{q,m_i}\Gamma_{\mu m_1 m_4\nu}(k-q)G_{m_1m_2}(q) \\ & \times\Delta_{m_2m_3}(q)G_{m_4m_3}(-q). \end{aligned} \tag{S8}$$

III. DISCUSSIONS ON THE SPIN SUSCEPTIBILITY

Here we provide discussions on the FLEX spin susceptibility of the four-orbital model. $\chi_S(\boldsymbol{q},0)$, given as the maximum eigenvalue of the spin susceptibility matrix at the lowest Matsubara frequency, is plotted in Fig. S3. For comparison, we also plot $\chi_S(\boldsymbol{q},0)$ for models (i) (interorbital interaction turned off) and (iii) (interorbital interaction and hybridization turned off). In the original model and model (i), there are relatively sharp peaks at $(\pm\frac{\pi}{2},\pm\frac{\pi}{2})$, while there is only a broad maximum around (π,π) in model (iii). This indicates that the peaks at $(\pm\frac{\pi}{2},\pm\frac{\pi}{2})$ originate from the hybridization between the two orbitals. In fact, the origin of these peaks have been identified in previous studies as the nesting between the $d_{3z^2-r^2}$ Fermi surface around (π,π) and the Fermi surface originating from the hybridization [S15]. On the other hand, in model (iii), there is no Fermi surface nesting among $d_{3z^2-r^2}$ bands since the antibonding $d_{3z^2-r^2}$

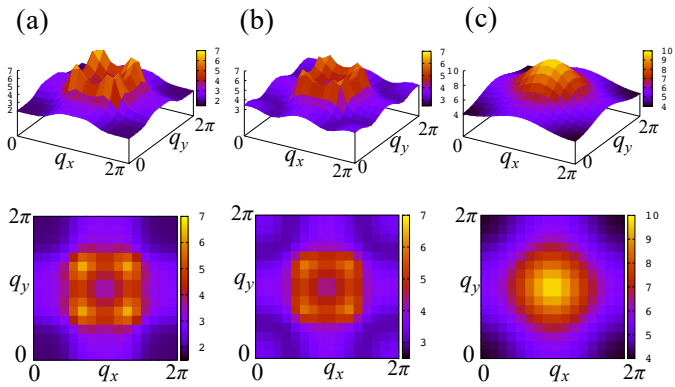

FIG. S3. Spin susceptibility $\chi_S(q_x, q_y, q_z = 0, i\omega_n = 0)$ obtained in FLEX. Panels (a), (b), and (c) correspond to the cases "original model", (i)(interorbital interaction turned off), and (iii)(interorbital interaction and orbital hybridization turned off) in table II of the main text, respectively. The bottom panels provide top views.

band does not intersect the Fermi level, but still, the interaction between bonding and antibonding bands gives rise to a broad maximum in the spin susceptibility at the wave vector (π, π), which is the vector that connects the Γ point, where the antibonding minimum is located, and (π, π), around which the bonding band forms a Fermi surface. From previous studies on the bilayer Hubbard model, it is known that such an interband interaction gives rise to finite energy spin fluctuations [S16]. As can be seen from the Eliashberg equation results for model (iii), it is this spin fluctuation that gives rise to the large eigenvalue for superconductivity. When the hybridization is turned on and the Fermi surface nesting sets in, the superconducting gap roughly maintains the structure of that of model (iii), and also the eigenvalue becomes smaller, indicating that the portion of the spin fluctuation that does not originate from the Fermi surface nesting plays the main role in the occurrence of the superconductivity.

IV. FURTHER ANALYSIS ON THE INTERORBITAL COUPLINGS

In the main text, we have seen that the interorbital couplings, namely, the one-body hybridization and the two-body interactions both degrade superconductivity. Here we further elaborate on this point. In Fig. S4(a), we plot λ for the original model and model (ii), i.e., the model without the interorbital hybridization, *against* $n[d_{3z^2-r^2}]$, namely, the average number of electrons per $d_{3z^2-r^2}$ orbitals, as we have done in Fig. 3(b) of the main text. It is found that the results of the two models are almost identical, indicating that the main origin of the suppression of superconductivity is the decrease of $n[d_{3z^2-r^2}]$, not the interorbital electron hoppings themselves. This further confirms our view that $n[d_{3z^2-r^2}]$ is an important factor for superconductivity. The importance of $n[d_{3z^2-r^2}]$ is consistent with a recent analysis on a two-orbital t-J ladder [S17].

As for the effect of the two-body interorbital interactions, we plot in Fig. S4(b), λ against Hund's coupling J, where only J is turned on while U' and J' are turned off. We find that J itself actually enhances superconductivity in a realistic parameter range, which can be considered as at least qualitatively consistent with recent works that study the effect of Hund's coupling [S17–S22].

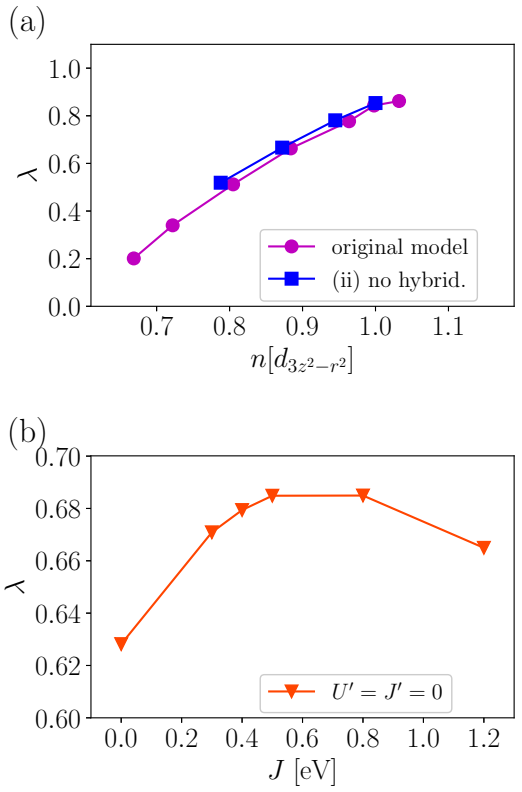

FIG. S4. (a) The eigenvalues λ of the linearized Eliashberg equation at $T = 0.01$ eV plotted against the average number of electrons per $d_{3z^2-r^2}$ orbitals $n[d_{3z^2-r^2}]$ for the original model and the model without the hybridization (see the main text for further explanation of the models). (b) λ is plotted against Hund's coupling J, where only J is turned on as an interorbital interaction, while U' and J' are turned off.

* sakakibara@tottori-u.ac.jp

[S1] H. Sun, M. Huo, X. Hu, J. Li, Y. Han, L. Tang, Z. Mao, P. Yang, B. Wang, J. Cheng, D.-X. Yao, G.-M. Zhang, and M. Wang, Nature **621**, 493 (2023).
[S2] L. Wang, Y. Li, S. Xie, F. Liu, H. Sun, C. Huang,

Y. Gao, T. Nakagawa, B. Fu, D. Bo, Z. Cao, R. Yu, S. I. Kawaguchi, H. Kobayashi, M. Wang, C. Jin, H. Mao, and H. Liu, (2023), arXiv:2311.09186.
[S3] B. Geisler, J. J. Hamlin, G. R. Stewart, R. G. Henning, and P. J. Hirshfeld, (2023), arXiv:2309.15078.
[S4] H. LaBollita, V. Pardo, M. R. Norman, and A. S. Botana, (2023), arXiv:2309.17279.
[S5] N. Marzari and D. Vanderbilt, Phys. Rev. B **56**, 12847 (1997).
[S6] I. Souza, N. Marzari, and D. Vanderbilt, Phys. Rev. B **65**, 035109 (2001).
[S7] RESPACK and its user guide can be downloaded from https://sites.google.com/view/kazuma7k6r.
[S8] K. Nakamura, Y. Yoshimoto, Y. Nomura, T. Tadano, M. Kawamura, T. Kosugi, K. Yoshimi, T. Misawa, and Y. Motoyama, Computer Physics Communications **261**, 107781 (2021).
[S9] K. Nakamura, Y. Nohara, Y. Yosimoto, and Y. Nomura, Phys. Rev. B **93**, 085124 (2016).
[S10] K. Nakamura, Y. Yoshimoto, T. Kosugi, R. Arita, and M. Imada, Journal of the Physical Society of Japan **78**, 083710 (2009).
[S11] K. Nakamura, R. Arita, and M. Imada, Journal of the Physical Society of Japan **77**, 093711 (2008).
[S12] Y. Nohara, S. Yamamoto, and T. Fujiwara, Phys. Rev. B **79**, 195110 (2009).
[S13] T. Fujiwara, S. Yamamoto, and Y. Ishii, Journal of the Physical Society of Japan **72**, 777 (2003).
[S14] The definition of energy window is shown in the user guide of RESPACK [S7].
[S15] Z. Luo, X. Hu, M. Wang, W. Wú, and D.-X. Yao, Phys. Rev. Lett. **131**, 126001 (2023).
[S16] M. Nakata, D. Ogura, H. Usui, and K. Kuroki, Phys. Rev. B **95**, 214509 (2017).
[S17] M. Kakoi, T. Kaneko, H. Sakakibara, M. Ochi, and K. Kuroki, (2023), arXiv:2312.04304.
[S18] X.-Z. Qu, D.-W. Qu, W. Li, and G. Su, (2023), arXiv:2311.12769.
[S19] K. Jiang, Z. Wang, and F.-C. Zhang, (2023), arXiv:2308.06771.
[S20] X.-Z. Qu, D.-W. Qu, J. Chen, C. Wu, F. Yang, W. Li, and G. Su, (2023), arXiv:2307.16873.
[S21] C. Lu, Z. Pan, F. Yang, and C. Wu, (2023), arXiv:2307.14965.
[S22] H. Oh and Y.-H. Zhang, Phys. Rev. B **108**, 174511 (2023).